99%-fidelity ballistic quantum-state transfer through long uniform channels

T. J. G. Apollaro,[1,2] L. Banchi,[3] A. Cuccoli,[4,5] R. Vaia,[6] and P. Verrucchi[4,5,6]

[1]*Dipartimento di Fisica, Università della Calabria, Via P. Bucci, 87036 Arcavacata di Rende (CS), Italy*

[2]*INFN-Gruppo collegato di Cosenza, Via P. Bucci, 87036 Arcavacata di Rende (CS), Italy*

[3]*ISI Foundation, Via Alassio 11/c, I-10126 Torino (TO), Italy*

[4]*Dipartimento di Fisica, Università di Firenze, Via G. Sansone 1, I-50019 Sesto Fiorentino (FI), Italy*

[5]*INFN Sezione di Firenze, via G. Sansone 1, I-50019 Sesto Fiorentino (FI), Italy*

[6]*Istituto dei Sistemi Complessi, Consiglio Nazionale delle Ricerche, via Madonna del Piano 10, I-50019 Sesto Fiorentino (FI), Italy*

(Received 25 March 2012; published 25 May 2012)

Quantum-state transfer with fidelity higher than 0.99 can be achieved in the ballistic regime of an arbitrarily long one-dimensional chain with uniform nearest-neighbor interaction, except for the two pairs of mirror-symmetric extremal bonds, say x (first and last) and y (second and penultimate). These have to be roughly tuned to suitable values $x \sim 2N^{-1/3}$ and $y \sim 2^{3/4}N^{-1/6}$, where N is the chain length. The general framework can describe the end-to-end response in different models, such as fermion or boson hopping models and XX spin chains.

DOI: 10.1103/PhysRevA.85.052319 PACS number(s): 03.67.Hk, 03.67.Pp, 03.67.Bg, 75.10.Pq

I. INTRODUCTION

Transferring quantum states between distant registers is one of the basic tasks that a quantum computer based on qubits located on fixed positions has to accomplish. The general scheme where a quantum channel physically connects the sending and the receiving qubits naturally emerges from such a requirement and a variety of proposals have been recently put forward for realizing quantum channels for state transmission by different physical solutions: phonon modes for trapped ions [1] or photon modes for superconducting qubits [2,3], molecular lattices for vibrational excitons [4] or optical lattices for cold atoms [5–8], arrays of coupled quantum dots [9–12], and interacting $S = \frac{1}{2}$ spins on a one-dimensional lattice, usually referred to as spin chains. In particular, proposals based on spin chains were first introduced in this context by Bose [13,14] and have attracted much attention in the last decade, due to both the possibility of exploiting their natural dynamics for the transfer process, and the availability of analytical results that allow for a detailed description of their dynamics.

All of the above-mentioned proposals are based on the idea that the state of the sender qubit be transferred at large distance via a dynamical site-to-site hopping mechanism that we will here describe in terms of a general *hopping model*. Once a two-dimensional Hilbert space, generated by $|0\rangle$ and $|1\rangle$, is assigned to each site $i = 1, \ldots, N$ of a one-dimensional lattice, the hopping model is defined by the following Hamiltonian:

$$\mathcal{H} = \frac{1}{2}\sum_{i,j=1}^{N} A_{ij}|\underline{i}\rangle\langle\underline{j}|, \tag{1}$$

where $|\underline{i}\rangle \equiv |0\rangle^{\otimes i-1}|1\rangle|0\rangle^{\otimes N-i}$ is a brief notation for single-excitation states. Indeed, when quasiperfect state transmission is considered, initial states with many excitations only slightly perturb the process, as we extensively analyzed in [15], so that in this paper we restrict the discussion to the single-excitation subspace. The structure of the hopping-amplitude matrix $\boldsymbol{A} = \{A_{ij}\}$ depends on the properties of the specific model and, despite being responsible of a possibly long-distance transfer process, it can be generated by a short-range interaction. Notice that Eq. (1) describes free bosons as well as free fermions and, as far as the latter are concerned, an exact mapping exists between the Hamiltonian (1) and that of the $S = \frac{1}{2}$ XY chain, where the matrix elements A_{ij} correspond to the exchange couplings. By the hopping model the basic transmission mechanisms can be studied and characterized: this, in turn, can also enlighten on the specific role of nonlinearity [16–18], noise [19], and dissipation [20,21].

The quality of the channel, as far as the transfer process is concerned, essentially depends on the hopping amplitudes A_{ij}; in particular, it has been proven that locally engineered hopping amplitudes can lead to perfect state transfer [22–28]. A recent proposal, aimed at improving the fidelity in the presence of disorder, deals with a combination of the above scheme and very weak extremal couplings [29]. However, strategies based on a very detailed design of the internal couplings appear very demanding from a practical point of view [30].

Having in mind that experimental setups generally require the couplings to be as uniform as possible (see, e.g., Ref. [31]), different authors have proposed alternative strategies for obtaining high-quality state-transfer processes through mirror-symmetric channels with uniform bulk and just a few extremal couplings allowed to vary [32–37]. Some of these alternative strategies are based on the idea of markedly weakening the couplings between the channel and the sender and receiver qubits, a solution that has been shown [32,34,38] to lead to a very-high-quality state transfer. However, this scheme yields large transmission times and requires such a reduction of the extremal bonds that a severe limitation on the actual length of a functioning channel must be taken into account.

In general, the transmission quality of almost-uniform channels is expected to deteriorate as the length of the channel is increased [13,14,36] due to dispersion, which is integral to uniformly distributed couplings. On the other hand, modeling a scalable quantum-state transfer process whose quality depends as little as possible on the physical length of the channel is an essential issue to address, especially if solid-state implementations and/or experimental analysis are in order.

Therefore, we find ourselves squeezed between the seemingly incompatible requirements of avoiding too much detailed

design of the physical channel and yet getting a reasonably long channel characterized by a relatively convenient transfer time.

Our approach to solve this puzzle stems from the idea of exploiting, in an almost uniform channel, the ballistic state-transfer mechanism that allows perfect transmission of a wave packet [35,39,40], in virtue of a perfectly coherent, nondispersive, dynamics. Perfect-transfer follows from the requirement that the normal modes correspond to equally spaced eigenfrequencies (or, loosely speaking, to a linear dispersion relation), so that a coherent mirrored reconstruction of all normal components occurs [41]. We infer that locally engineering all the interactions in order to yield a linear spectrum is not necessary as only the modes involved in the initial configuration of the overall system need to satisfy the linearity condition [35] in order to get an effectively ballistic dynamics: systems realizing this condition can be dubbed "optimal state-transfer" systems. They realize coherent ballistic transmission in spite of the dispersion relation not being linear in the whole range, but only in the neighborhood of the normal modes excited by the initialization of the state of the first qubit, which coherently evolve as a traveling wave packet that rebuilds the state at the opposite end.

This idea has been proposed and implemented [15,35] in a scheme where we could only play with one parameter of the Hamiltonian; namely, the value of the extremal bond $x = A_{12} = A_{N-1,N}$. We learned that the emergence of an optimal value for x follows from quite a complex interplay between two conflicting effects, i.e., the deformation of the eigenvalue spacings and the shrinking of the mode distribution, which are simultaneously driven by the value of x. In order to further improve our results, we understand that these effects must be handled independently: a goal that be accomplished by introducing just one more parameter in the model, as shown in this paper. Notice that the introduction of a second parameter in the model should not be thought of as a way of moving towards the perfect-transfer scheme (which requires $N/2$ parameters) but rather as a practical answer to the effective need to control two competing effects.

In Sec. II the state-transfer mechanism in the hopping model (1) is studied and the quantities that characterize the efficiency of the quantum channel in terms of the transition amplitudes are obtained. In Sec. III we describe the setup for implementing the two-parameter optimal-transfer scheme (with two adjacent modified bonds at the ends of the chain) and derive implicit analytical expressions for the frequencies and the matrix elements entering the transition amplitude. The behavior of the latter is thoroughly discussed in Sec. IV, where numerical results are reported together with the analytical derivation of the large-N limit of the attainable optimal transmission fidelity. In Sec. V the dynamical behavior is shown to be ballistic, i.e., the information is carried by a wave packet traveling at constant speed along the channel. Conclusions are drawn in Sec. VI. Some details of the calculations are reported in Appendix A.

II. STATE TRANSFER IN HOPPING MODEL

Let us consider the Hamiltonian (1). In the case of nearest-neighbor interactions the matrix $\boldsymbol{A}$ is tridiagonal and, for the chain to be connected, the off-diagonal elements cannot vanish. Without loss of generality [42], we assume $\boldsymbol{A}$ to be real with $A_{i,i+1} = A_{i+1,i} > 0$. Introducing the orthogonal matrix $\boldsymbol{U} = \{U_{ni}\}$ that diagonalizes the matrix A,

$$\sum_{ij} U_{ni} A_{ij} U_{mj} = \lambda_n \delta_{nm} \equiv 2\omega_n \delta_{nm}, \tag{2}$$

and the one-excitation states

$$|\underline{n}\rangle = \sum_i U_{ni} |\underline{i}\rangle, \tag{3}$$

the Hamiltonian takes the diagonal form

$$\mathcal{H} = \sum_{n=1}^{N} \omega_n |\underline{n}\rangle\langle\underline{n}|. \tag{4}$$

If $\boldsymbol{A}$ commutes with the mirroring matrix $\boldsymbol{J} = \{J_{ij} = \delta_{N+1-i,j}\}$, (i.e., $\boldsymbol{A}$ is mirror symmetric), then also $\boldsymbol{J}$ is diagonalized by $\boldsymbol{U}$,

$$\sum_j J_{ij} U_{nj} = U_{n,N+1-i} = j_n U_{ni}, \tag{5}$$

and since $\boldsymbol{J}^2 = 1$ the eigenvalues j_n are either 1 or -1. It is proved in Ref. [43] that, if the eigenvalues ω_n are cast in decreasing order, then $j_n = (-)^{n+1} = -e^{i\pi n}$; in other words, the nth eigenvector of $\boldsymbol{A}$ is mirror symmetric or mirror antisymmetric according to whether n is odd or even, respectively.

A. Estimating state-transfer quality

The purpose of state transfer is to start with a product state $|\underline{\psi}\rangle = |\psi\rangle|0\rangle^{\otimes N-1}$, with a generic state

$$|\psi\rangle = \alpha|0\rangle + \beta|1\rangle \tag{6}$$

of the first qubit and let it evolve with $\mathcal{H}$ in such a way that, at a given time $t \simeq N$ the state of the last qubit is as close as possible to $|\psi\rangle$. Formally, the evolved overall state is $\rho(t) = e^{-i\mathcal{H}t}|\underline{\psi}\rangle\langle\underline{\psi}|e^{i\mathcal{H}t}$ and the instantaneous state at site i is

$$\rho_i(t) = \mathrm{Tr}_{\{1,\ldots,i-1,i+1,\ldots,N\}}\rho(t). \tag{7}$$

Defining $|\underline{0}\rangle = |0\rangle^{\otimes N}$, the evolved overall state obeys

$$e^{-i\mathcal{H}t}|\underline{\psi}\rangle = \alpha|\underline{0}\rangle + \beta\sum_i \langle\underline{i}|e^{-i\mathcal{H}t}|\underline{1}\rangle|\underline{i}\rangle, \tag{8}$$

so that

$$\rho_i(t) = \begin{bmatrix} 1-|\beta|^2|u_i(t)|^2 & \alpha\beta^* u_i^*(t) \\ \alpha^*\beta u_i(t) & |\beta|^2|u_i(t)|^2 \end{bmatrix}, \tag{9}$$

where $u_i(t)$ is the transition amplitude from site 1 to site i,

$$u_i(t) \equiv \langle\underline{i}|e^{-i\mathcal{H}t}|\underline{1}\rangle = \sum_{n=1}^{N} U_{ni}U_{n1}e^{-i\omega_n t}. \tag{10}$$

The state of the last qubit is described by the density matrix $\rho_N(t)$, whose degree of similarity with the initial state $|\psi\rangle\langle\psi|$ can be estimated by the fidelity,

$$\mathcal{F}(\psi,t) = \langle\psi|\rho_N(t)|\psi\rangle. \tag{11}$$

The overall channel quality can be estimated by taking the average of $F(\psi,t)$ over all possible initial states $|\psi\rangle$ (i.e., over

the Bloch sphere, $|\alpha|^2+|\beta|^2=1$). This yields the average fidelity $\mathcal{F}(t)$ in terms of $u_N(t)$, with a dependence on the phase of the amplitude that one can get rid of by prescribing a proper local rotation to the last qubit [15], or, in a spin-chain context, by applying a suitable magnetic field [13] in such a way that $u_N(t)$ is real and positive at the arrival time. With this proviso, setting

$$u(t)\equiv|u_N(t)|, \tag{12}$$

one has

$$\mathcal{F}(t)=\frac{1}{3}+\frac{[1+u(t)]^2}{6}. \tag{13}$$

Hence, the average fidelity is a monotonic function of (the modulus of) the transition amplitude $u(t)$. On the same footing, it can be shown that the entanglement fidelity, which measures the efficiency of transfer for an entangled state with an external noninteracting qubit, reads [15]

$$\mathcal{F}_{\mathrm{E}}(t)=\frac{[1+u(t)]^2}{4}. \tag{14}$$

It is clear at this point that $u(t)\in[0,1]$ can be assumed as a transfer-quality indicator, with $u(t)=1$ corresponding to perfect transfer. For almost perfect transfer, $u=1-\varepsilon$, one has a reduction of the fidelity to first order in ε,

$$\mathcal{F}\approx 1-\tfrac{2}{3}\varepsilon,\quad \mathcal{F}_{\mathrm{E}}\approx 1-\varepsilon. \tag{15}$$

In the following we will thus concentrate onto the task of maximizing the transition amplitude $u(t)$ for the particular model introduced in the next section.

B. Mirror-symmetric case

If $\boldsymbol{A}$ is mirror symmetric, Eq. (5) tells us that $U_{nN}=-e^{i\pi n}U_{n1}$, so the transition amplitude we are interested in takes the form

$$u(t)=\left|\sum_{n=1}^{N}\mathcal{P}_n e^{i(\pi n-\omega_n t)}\right|,\quad \mathcal{P}_n\equiv U_{n1}^2, \tag{16}$$

which consists of a sum of time-evolving phases with a weight given by the mode distribution (or density) $\mathcal{P}_n$. In the case of equally spaced eigenfrequencies $\omega_n=\omega_0+v(\pi/N)n$, where v is a constant, one would have $u(t=N/v)=1$ (i.e., full transmission of the state). As already mentioned in the introduction, this case of a "linear dispersion" can be realized in discrete finite systems [24] by allowing any single nearest-neighbor coupling to be properly tuned such that $A_{i,i+1}\propto\sqrt{i(N-i)}$.

III. THE QUASIUNIFORM CHANNEL

In a quasiuniform chain almost all couplings are equal, setting a natural energy unit and, taking the chain spacing as the length unit, all quantities reported in the following become dimensionless; for instance, if the bulk dimensionful coupling is J and the dimensionful lattice spacing is d, then energies are in units of J, times in units of $\hbar/J$, velocities in units of $dJ/\hbar$, and so on.

We assume from now on that the mirror-symmetric matrix $A=\{A_{ij}\}$ describes the chain of Fig. 1, which is uniform

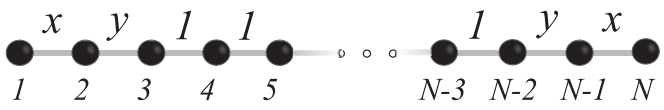

FIG. 1. Mirror-symmetric quantum channel consisting of N sites with uniform bonds of unit strength, except for two pairs of weaker bonds at the extrema, x and y. State transmission is meant to occur between sites 1 and N.

except for the two extremal bonds $A_{1,2}=A_{N-1,N}\equiv x$ and $A_{2,3}=A_{N-2,N-1}\equiv y$, while all other couplings are equal, $A_{i,i+1}=1$ for $i=3,\ldots,N-3$. Such quasiuniform interactions were used in Refs. [8,44] for the purpose of studying long-distance entanglement in the ground state. Explicitly,

$$A(x,y)=\begin{pmatrix}
0 & x & & & & & & \\
x & 0 & y & & & & & \\
 & y & 0 & 1 & & & & \\
 & & 1 & 0 & 1 & & & \\
 & & & \ddots & \ddots & \ddots & & \\
 & & & & 1 & 0 & y & \\
 & & & & & y & 0 & x \\
 & & & & & & x & 0
\end{pmatrix}. \tag{17}$$

It is assumed that $0<x\leqslant 1$ and $0<y\leqslant 1$. In Appendix A the N energy eigenvalues are found in the form $\omega_n=\cos k_n$, where the allowed values $k=k_n$ are determined by Eqs. (A12) and (A13), and the mode distribution $\mathcal{P}_k$ is given by Eq. (A23). As the latter is symmetric around $\pi/2$, it is more convenient to work with the shifted variable

$$q\equiv\frac{\pi}{2}-k\in\left(-\frac{\pi}{2},\frac{\pi}{2}\right), \tag{18}$$

whose allowed values are

$$q_m=\frac{\pi m-2\varphi_{q_m}}{N+1},\quad m=-\frac{N-1}{2},\ldots,\frac{N-1}{2}, \tag{19}$$

where $m\equiv(N+1)/2-n$; the corresponding eigenfrequencies are $\omega_q=\sin q$. Understanding that the variable q assumes the allowed values (19), we can use it in the place of the eigenvalue index n. Note that, for even N, m is half integer, but there is no qualitative difference between the outcomes for even and odd N: the latter case is just more easily handled numerically. The *phase shifts*

$$\varphi_q=\tan^{-1}\left[\frac{y^2\sin 2q}{x^2-(2-y^2)(1-\cos 2q)}\right]-2q \tag{20}$$

displace the q values from the equally spaced values of the fully uniform case ($\varphi_q=0$ for $x=y=1$). Note that the phase shifts do not alter the order of the sequence $\{q_m\}$.

Note that the denominator of Eq. (20) can vanish and the argument of $\tan^{-1}$ can jump from ∞ to $-\infty$: when this happens, the conventional range of $\tan^{-1}$ has to be extended above $\pi/2$ rather than jumping from $\pi/2$ to $-\pi/2$. In this way φ_q is a continuous function, shown in Fig. 2 for positive q. The effect of weakening the bond y is evident: the deformation is such that φ_q changes its convexity in an interval $|q|\lesssim q_{\mathrm{F}}(x)$ whose width is characterized by the fixed point $q_{\mathrm{F}}(x)=\sin^{-1}\frac{x}{2}$. Therefore, the parameter y can change

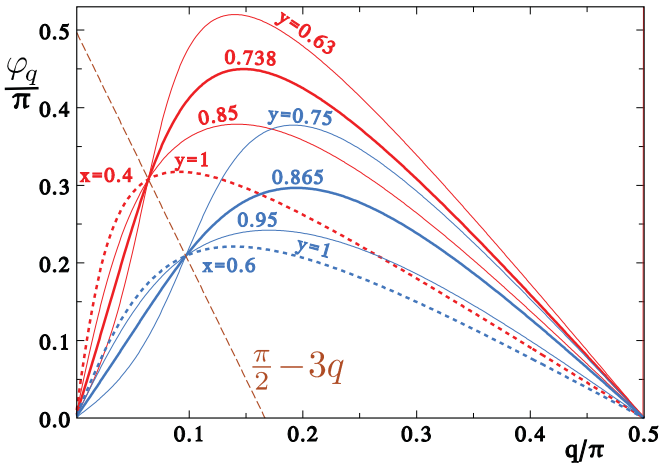

FIG. 2. (Color online) Shifts φ_q [Eq. (20)] for different values of x and y. The dashed curves correspond to $y = 1$. The fixed point $q_F = \sin^{-1}\frac{x}{2}$ lies on the dashed straight line.

the separation between the allowed q values and, in turn, between the eigenfrequencies affecting the coherence in the time evolution.

The mode distribution $\mathcal{P}_k = U_{k1}^2$, Eq. (A23), can be written in terms of q as

$$\mathcal{P}_q = \frac{2}{N+1+2\varphi_q'} \times \frac{x^2 y^2}{x^4 + (4-x^2-2y^2)^2 \tan^2 q - 16(1-y^2)\sin^2 q}. \quad (21)$$

The term in φ_q' is clearly irrelevant for a long chain, even though it ensures the normalization, $\sum_m \mathcal{P}_{q_m} = 1$, for any finite N. Figure 3 describes the typical behavior of the mode density $\mathcal{P}_q$ when y is varied keeping a fixed $x < 1$. Compared to its counterpart in the case of the uniform chain, $x = y = 1$,

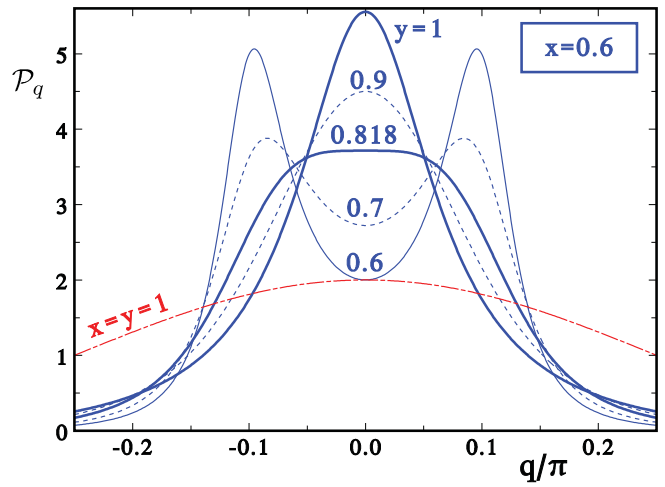

FIG. 3. (Color online) Normalized large-N mode density $\mathcal{P}_q$ [Eq. (21)] for $x = 0.6$ and different values of the second bond coupling y. The thicker curves are those for $y = 1$ and for the threshold value $y = Y(x)$ (see text and Fig. 4). The broad dash-dotted line is the result for the fully uniform chain, $x = y = 1$.

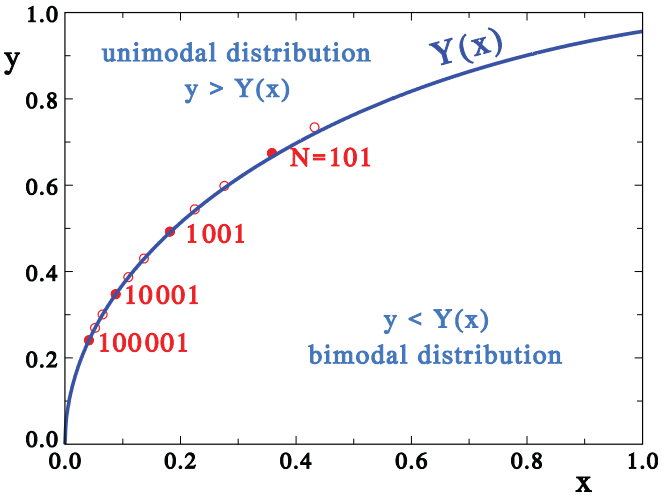

FIG. 4. (Color online) Function $Y(x)$ [Eq. (22)] separates the occurrence of unimodal and bimodal mode distributions. The optimized pairs (x, y) [i.e., those which maximize the arrival amplitude $u(t)$], are also reported for selected values of N (see Table I).

it is evidently more structured; by lowering y its tails get increasingly suppressed and $\mathcal{P}_q$ definitely changes to a bimodal shape with two symmetric maxima: this occurs when, in the denominator, the coefficient of $\sin^2 q$ becomes larger than that of $\tan^2 q$; that is, when y is smaller than

$$Y(x) \equiv \sqrt{\sqrt{2}x - \frac{x^2}{2}}, \quad (22)$$

which is the curve shown in Fig. 4. $\mathcal{P}_q$ is unimodal for $y \geqslant Y(x)$ and has its maximum at $q = 0$; at the threshold $y = Y(x)$ the maximum flattens, the deviation being $\sim q^4$, before developing the lateral maxima which are the more pronounced the smaller y. In the limit $y \to 0$ the distribution $\mathcal{P}_q$ tends to two symmetric δ peaks at $q = \pm\sin^{-1}\frac{x}{2}$, corresponding to the excitations of the single dimer with interaction x, which is indeed isolated from the chain when $y = 0$.

To represent the behavior of the level spacings, whose uniformity is crucial for the coherence of transmission, one can define a sort of "group velocity" by

$$v_q \equiv \frac{N+1}{\pi}\omega_q' \partial_m q = \frac{N+1}{N+1+2\varphi_q'}\cos q, \quad (23)$$

where the "derivative" of Eq. (19), $(N+1+2\varphi_q')\partial_m q = \pi$, has been used, and from Eq. (20),

$$\varphi_q' = -2 + \frac{2y^2[x^2 + 2(2-x^2-y^2)\sin^2 q]}{x^4 + 4[y^4 - x^2(2-y^2)]\sin^2 q + 16(1-y^2)\sin^4 q}. \quad (24)$$

IV. TRANSITION AMPLITUDE

A. Numerical results

The transition amplitude between the sites 1 and N at the time t is given by Eq. (16). It can conveniently be rewritten as a sum over the allowed q values (19),

$$u(t) = \left| \sum_m \mathcal{P}_{q_m} e^{i(\pi m - t \sin q_m)} \right|. \quad (25)$$

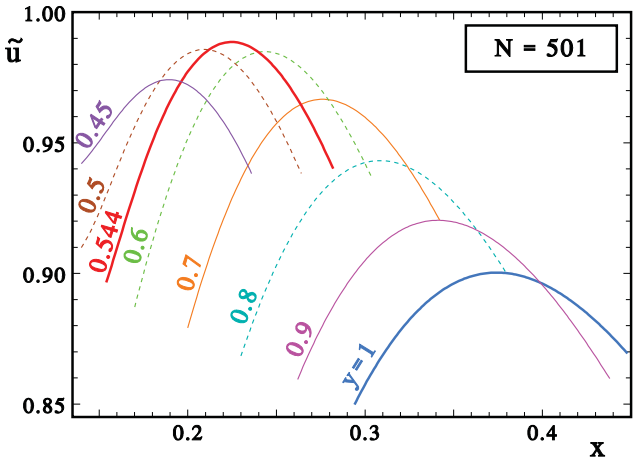

FIG. 5. (Color online) End-to-end amplitude $\tilde{u}(x,y)$ at arrival time as a function of x for selected values of y and $N = 501$. The thicker curves correspond to $y = 1$ and to the optimized value $y = 0.5439$.

This sum can be evaluated numerically: for any pair (x,y) our code solves iteratively the coupled Eqs. (19) and (20) and looks for the value of the arrival time $t \gtrsim N$ when $u(t)$ attains its largest value, say $\tilde{u}(x,y)$. Typical results for $\tilde{u}(x,y)$ are reported as a function of x for selected values of y in Fig. 5, which refers to a chain of length $N = 501$. One can see that taking y smaller than 1 the amplitude can become much closer to 1, also for the longest channels, and it is possible to identify the optimal values $(x^{\rm opt}, y^{\rm opt})$ that make $\tilde{u}(x,y)$ reach its maximum $u^{\rm opt} \equiv \tilde{u}(x^{\rm opt}, y^{\rm opt})$. Moreover, the maxima are so broad in the (x,y) plane that a relatively large mismatch from the optimal values still keeps giving a large amplitude, and consequently a large average transmission fidelity, as can be appreciated in the contour plots of Figs. 6 and 7.

The numerically evaluated optimal data are reported in Table I, together with those obtained in Ref. [15] by varying only x with $y = 1$. Comparing with the latter, it is seen that the transfer quality improves in an extraordinary way: even for

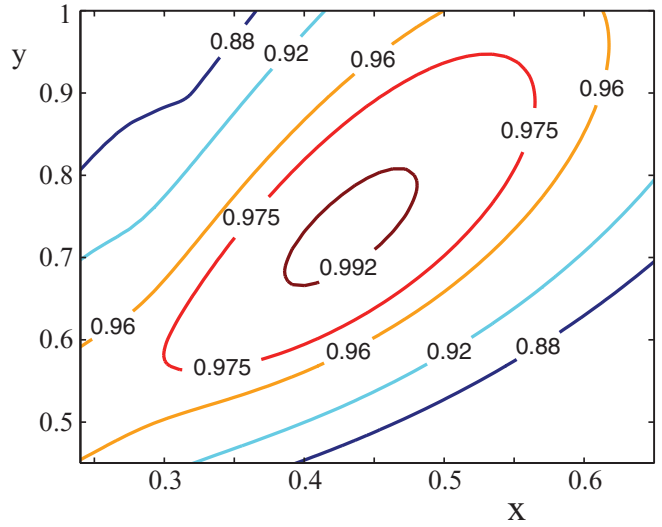

FIG. 6. (Color online) Contour plot of the average fidelity $\mathcal{F}(x,y)$ at arrival time in (x,y) plane for $N = 51$.

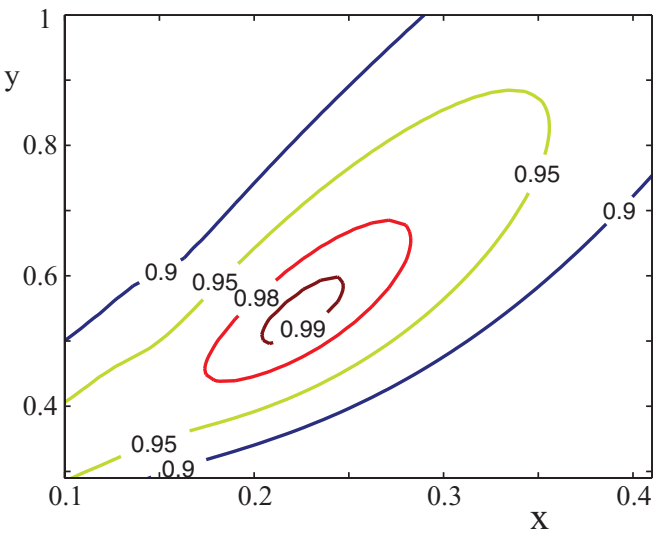

FIG. 7. (Color online) Contour plot of the average fidelity $\mathcal{F}(x,y)$ at arrival time in (x,y) plane for $N = 501$.

a chain of length $N = 50\,001$ the amplitude increases from 0.859 to 0.987; that is, the state-transfer fidelity $\mathcal{F}$ rises from 0.909 to 0.991. The values of Table I show that the optimized transmission amplitude decreases more and more weakly for large N, so that there could be a finite asymptotic amplitude attainable for an infinite chain: this is the case, indeed, as shown in the next subsection. In Fig. 8 the optimal values for x are reported for $y = 1$ and for $y = y^{\rm opt}$. As shown formally in the next subsection, it turns out that $x^{\rm opt}$ scales as $N^{-1/6}$ in the former case, while it obeys a new scaling law, apparently $N^{-1/3}$, in the latter.

The great improvement in transmission quality deals with the same argument we gave in Ref. [15]: although a constant group velocity v_q yields perfect transmission, it is sufficient that v_q be constant for the q modes excited by the initialization of the first qubit whose distribution is $\mathcal{P}_q$. The results illustrated above confirm that the possibility of controlling, by means of *two* parameters (x and y), the *two* most relevant features, shape of $\mathcal{P}_q$ and stability of v_q, allows us to obtain an optimal tradeoff leading to nearly perfect transmission.

The weaker second bond y acts indeed on the group velocity, as appears in Fig. 9, where the shape of v_q is reported for the optimized value of x and compared with the corresponding mode density $\mathcal{P}_q$. With a smaller y, the central dip appearing for $y = 1$ is strongly reduced and the group velocity just shows a small modulation in a rather wide range, so favoring a coherent dynamics; at the same time $\mathcal{P}_q$ broadens, but not dramatically as it is mainly controlled by x (see, e.g., Fig. 4 of Ref. [15]); the optimized value $y = y^{\rm opt}$ clearly gives the best result compatible with the assumed parametrization.

B. Asymptotic behavior for large N

The numerically estimated optimal pairs $(x^{\rm opt}, y^{\rm opt})$ are shown in Fig. 4. They evidently lie almost exactly on the threshold curve $Y(x)$ separating the unimodal from the doubly peaked shape of $\mathcal{P}_q$, i.e., $y^{\rm opt} \simeq Y(x^{\rm opt})$. We expect this to hold in the large-N regime, since the condition $y = Y(x)$ clears the quadratic terms in the denominator of the density (21) leaving smaller tails $\sim q^{-4}$, thus allowing for a more effective cut of

TABLE I. Optimal pairs $(x^{\rm opt}, y^{\rm opt})$, corresponding amplitude $u^{\rm opt} = \tilde{u}(x^{\rm opt}, y^{\rm opt})$, and average fidelity $\mathcal{F}^{\rm opt}$ for different channel lengths N. Also reported are the optimal values obtained in Ref. [15] with $y = 1$.

N	$x^{\rm opt}$	$y^{\rm opt}$	$u^{\rm opt}$	$\mathcal{F}^{\rm opt}$	$x^{\rm opt}(y=1)$	$u^{\rm opt}(y=1)$	$\mathcal{F}^{\rm opt}(y=1)$
51	0.4322	0.7338	0.99270	0.99514	0.5542	0.9493	0.9666
101	0.3584	0.6742	0.99091	0.99395	0.4931	0.9324	0.9557
251	0.2760	0.5982	0.98932	0.99290	0.4216	0.9127	0.9431
501	0.2247	0.5439	0.98855	0.99239	0.3742	0.9003	0.9352
1001	0.1818	0.4923	0.98849	0.99235	0.3322	0.8899	0.9286
2501	0.1367	0.4300	0.98765	0.99179	0.2840	0.8791	0.9218
5001	0.1097	0.3869	0.98747	0.99167	0.2523	0.8726	0.9178
10 001	0.0878	0.3474	0.98735	0.99159	0.2242	0.8674	0.9145
25 001	0.0652	0.3004	0.98726	0.99153	0.1920	0.8621	0.9112
50 001	0.05209	0.26925	0.98722	0.99151	0.1708	0.8590	0.9093
100 001	0.04150	0.24072	0.98720	0.99149	0.1519	0.8565	0.9078
$N \to \infty$	$1.954\ N^{-1/3}$	$1.662\ N^{-1/6}$	0.98715	0.99146	$1.030\ N^{-1/6}$	0.8469	0.9018

the modes involving the main nonlinear part of v_q. Therefore, instead of considering y as a free parameter, we fix it to be given by

$$y \equiv Y(x) = \sqrt{\sqrt{2}x - \frac{x^2}{2}} = 2^{1/4}x^{1/2} + O(x^{3/2}). \tag{26}$$

As $N \to \infty$ the sum (25) can be written as an integral,

$$u_\infty(t) = \lim_{N\to\infty} \int dm \mathcal{P}_{q_m} e^{i(\pi m - t \sin q_m)}. \tag{27}$$

In order to evaluate this asymptotic expression, first note that from (19) that one has to set $\pi m = (N+1)q_m + 2\varphi_{q_m}$ and $\pi dm = (N + 1 + 2\varphi_q')dq$, so that

$$u_\infty(t) = \lim_{N\to\infty} \int_{-\frac{\pi}{2}}^{\frac{\pi}{2}} \frac{dq}{\pi} \tilde{\mathcal{P}}_q e^{i[(N+1)q + 2\varphi_q - t \sin q]}, \tag{28}$$

where

$$\tilde{\mathcal{P}}_q = \frac{2x^2y^2}{x^4 + (4 - x^2 - 2y^2)^2 \tan^2 q - 16(1-y^2)\sin^2 q} \tag{29}$$

is exactly the normalized function reported in Fig. 3. As, by increasing N, the optimal distribution gets narrower and narrower, the denominator can be expanded taking into account the assumption (26):

$$\tilde{\mathcal{P}}_q \simeq \frac{2^{3/2}x^3}{x^4 + (2q)^4}; \tag{30}$$

hence, the width of the relevant q region shrinks with x. Let us introduce the scaled variable $\xi = 2q/x$, which is of order unity, so that

$$\tilde{\mathcal{P}}_q dq \simeq \frac{\sqrt{2}d\xi}{1+\xi^4}. \tag{31}$$

As for the phase in Eq. (28), the leading term of the expansion of Eq. (20) is

$$\varphi_q \simeq \tan^{-1} \frac{\sqrt{2}\xi}{1-\xi^2} \tag{32}$$

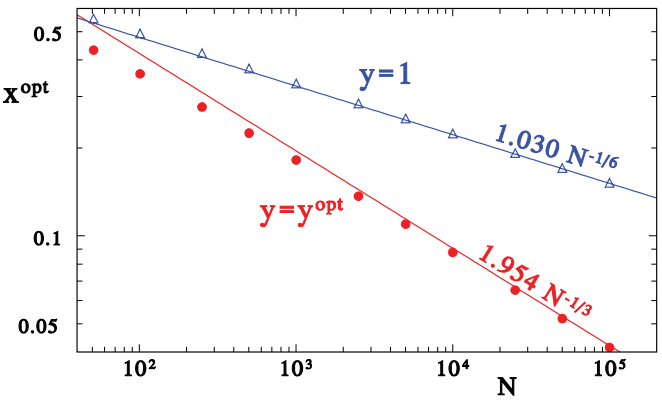

FIG. 8. (Color online) Optimal values for x, from Table I, reported vs N both for $y = 1$ and for the optimized $y = y^{\rm opt}$. Note that $x \sim N^{-1/6}$ in the former case, while $x \sim N^{-1/3}$ in the latter.

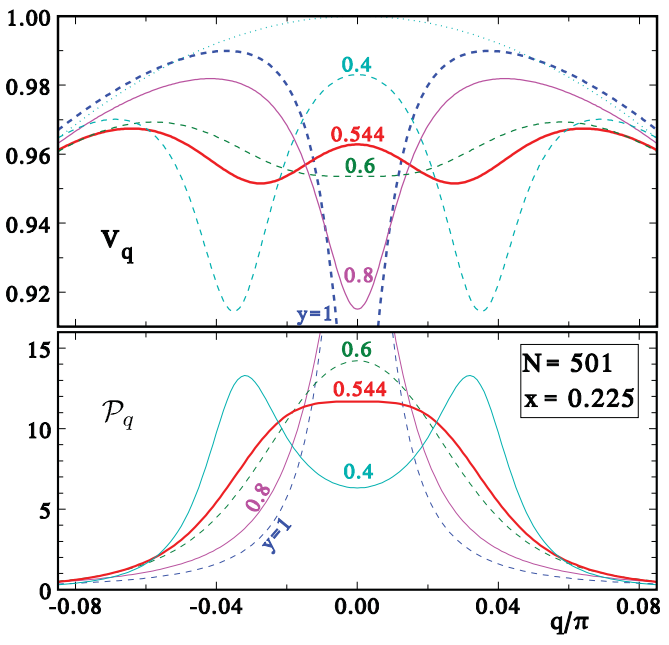

FIG. 9. (Color online) Group velocity v_q and corresponding mode density $\mathcal{P}_q$ for $N = 501$, $x = x^{\rm opt} = 0.225$, and selected values of y. The thicker curves correspond to $y = 1$ (dotted) and to the optimized value $y = y^{\rm opt} = 0.544$ (solid).

and, defining the arrival-time delay s by $t \equiv N+1+s$, the remaining terms read

$$(N+1)q - t\sin q = t(q-\sin q) - sq \simeq \tau\xi^3 - \sigma\xi, \quad (33)$$

where

$$\tau \equiv \frac{1}{6}\left(\frac{x}{2}\right)^3 t, \quad \sigma \equiv \frac{x}{2}s, \quad (34)$$

are the rescaled counterparts of the arrival time $t \sim N$ and delay $s \sim N^{1/3}$. Eventually, the asymptotic value of the amplitude reads

$$u_\infty(\tau,\sigma) = \frac{\sqrt{2}}{\pi}\int_{-\infty}^{\infty} d\xi \frac{\exp[i(\tau\xi^3 - \sigma\xi + 2\tan^{-1}\frac{\sqrt{2}\xi}{1-\xi^2})]}{1+\xi^4}. \quad (35)$$

For a numerical evaluation it is convenient to perform the substitution $\xi = \tan z$, and consider the maximization of

$$u_\infty = \frac{2\sqrt{2}}{\pi}\int_0^{\frac{\pi}{2}} dz \frac{1+\tan^2 z}{1+\tan^4 z}\cos\Phi(z), \quad (36)$$

with

$$\Phi(z;\tau,\sigma) = \tau\tan^3 z - \sigma\tan z + 2\tan^{-1}\frac{\tan 2z}{\sqrt{2}}. \quad (37)$$

Although this phase strongly oscillates for z close to $\pi/2$, the weighting function makes the numerical convergence easy. The overall maximum corresponds to $(\tau,\sigma) = (0.155\,45, 3.1645)$, and amounts to $u_\infty = 0.987\,153$, which is the asymptotic value reported in Table I together with the asymptotic scaling resulting from Eq. (34),

$$x^{\rm opt} \simeq 2\left(\frac{6\tau}{N}\right)^{1/3} \simeq 1.954N^{-1/3},$$
$$y^{\rm opt} = Y(x^{\rm opt}) \simeq 1.662N^{-1/6}, \quad (38)$$

while the delay scales as $s = 2\sigma/x \simeq 3.239N^{1/3}$, so that the arrival time is

$$t \simeq N + 1 + 3.239N^{1/3}. \quad (39)$$

V. STATE-TRANSFER DYNAMICS

In Sec. II we introduced the instantaneous transition amplitude from site 1 to any site i of the chain [Eq. (10)]. This quantity tells substantially where the information concerning the initial quantum state sits at any time t. Indeed, it obeys the sum rule

$$\sum_i |u_i(t)|^2 = \sum_{n=1}^{N} U_{n1}^2 = 1, \quad (40)$$

so one can view the state-transfer process as the transmission of a traveling wave packet of amplitude $u_i(t)$ which is able to optimally rebuild most of its content in the single Nth site. Looking at the dynamics of this wave packet sheds further light onto the ballistic transfer mechanism and allows for interesting comparisons based on the data for $|u_i(t)|$ reported in Figs. 10 and 11.

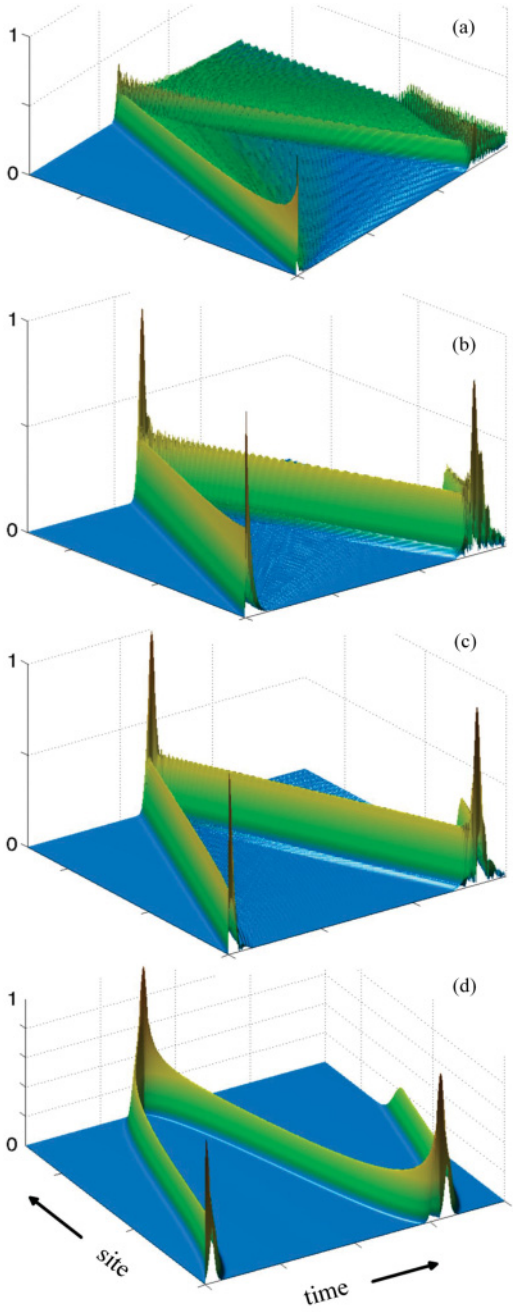

FIG. 10. (Color online) Space-time perspective views of the propagating wave packet $|u_i(t)|$ [Eq. (10)], for a chain of length $N = 251$, (a) in the fully uniform chain $x = y = 1$, (b) in the case $y = 1$ and optimal $x = 0.422$ [15], (c) in the quasiuniform channel [Eq. (17)], with the optimal $x = 0.276$ and $y = 0.598$, and (d) in the perfect-transfer channel [24] [Eq. (41)]. In all panels the site variable goes from 1 to 251 and the time variable from 0 to 600, as in Fig. 11.

The first comparison is made in panels (a), (b), and (c) of Figs. 10 and 11 and involves (a) the fully uniform channel, which displays a very dispersive dynamics and is indeed inefficient for transmission, (b) the channel with only one optimized extremal bond [15], showing an increased coherence, and (c) the further step with two optimized extremal couplings which improves transmission close to perfection. These features can be appreciated looking at the height of the

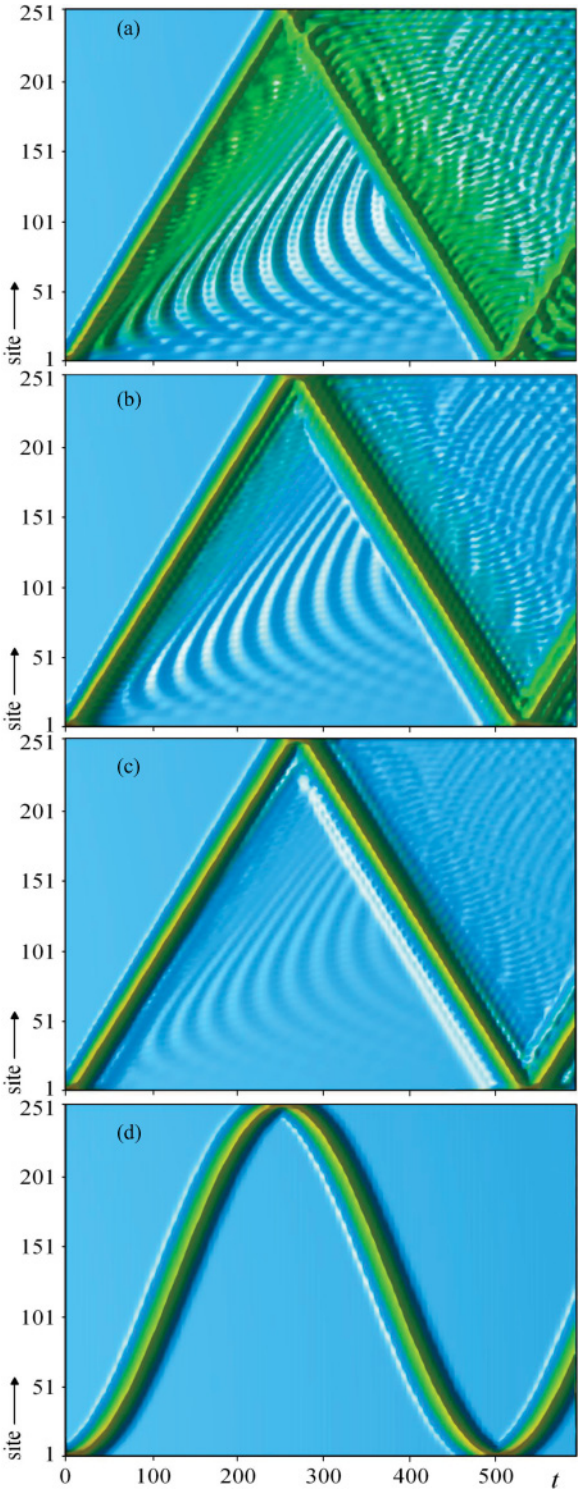

FIG. 11. (Color online) Space-time contour views of the propagating wave packet $|u_i(t)|$ [Eq. (10)] for the same cases as Fig. 10.

arrival-time maxima in Fig. 10 and at the the rugged features, more evident in Fig. 11, that represent the amplitude losses due to dispersion according to Eq. (40). Figure 11 makes also evident the increasing arrival delay from (a) to (b) and to (c) as a consequence of the slower packet injection and reconstruction due to the softened endpoint couplings.

Eventually, let us consider the case of perfect state transfer [24], which is obtained by designing all nearest-neighbor couplings along the chain proportionally to the height of a semicircle of diameter N drawn over the chain,

$$A_{i,i+1} = A_{i+1,i} = \frac{\pi}{N+1}\sqrt{i(N-i)}; \tag{41}$$

the energy unit being arbitrary, it is chosen here such that the resulting linear spectrum

$$\omega_m = \frac{\pi}{N+1}m, \quad m = -\frac{N-1}{2}, \ldots, \frac{N-1}{2}, \tag{42}$$

yields the exact arrival time $t = N+1$. Notice that, neglecting terms $\sim N^{-1}$, the maximum of the couplings $\{J_i\}$ is $\pi/2$, their average is $\pi^2/8$, and their mean-square value is $\pi/3$; this allows for a meaningful comparison with our model, and the corresponding data are reported in Figs. 10(d) and 11(d). The modulated couplings determine a varying velocity of the wave packet along the chain, at variance with its constant velocity in the uniform channel of panels Figs. 10(a)–10(c) and 11(a)–11(c).

VI. CONCLUSIONS

We have shown that almost perfect ballistic quantum-state transfer with fidelity larger than 0.99 can be obtained in an unmodulated channel of arbitrary length N just by allowing the two endpoint pairs of nearest-neighbor interactions, x and y, to assume optimal values $(x^{\mathrm{opt}}, y^{\mathrm{opt}})$. In addition, this maximum of the transmission quality in the (x,y) plane, as measured by the average fidelity or equivalently by the transition amplitude (16), is so broad that an experimental realization would not be bound to a fine-tuning of the endpoint couplings, as Figs. 6 and 7 clearly show.

One might think that the approach presented here looks like the second step of a sequence that, by allowing further bonds to vary, would lead to perfect ballistic transmission as found in Ref. [24]. However, such deduction does not hold true: indeed, while the aim of Ref. [24] is that of obtaining perfect transfer by letting all normal modes evolve coherently, here we look for high-quality transfer by requiring that only the modes excited by the initialization of the first qubit be able to evolve coherently. This is done within an effective scheme ruled by two effects; namely, the mode distribution and the frequency spacings, which can be kept under control by just two parameters: the extremal couplings x and y. Our approach leads to extremal couplings $x \sim N^{-1/3}$ and $y \sim N^{-1/6}$, sensibly larger than those required for perfect transfer [Eq. (41)] which scale as $N^{-1/2}$.

Furthermore, the value of the fidelity attainable with only two modified end bonds is so high (more than 0.99) that, *for all practical purposes*, the considerably more difficult task of engineering all the couplings would be unnecessary, because the unavoidable presence of imperfections in laboratory implementations would prevent perfect state transfer and, when the presence of disorder in the couplings along the chain is taken into account, it has been shown that the one-parameter optimal state-transfer scheme ($y = 1$) is more robust than the perfect-transfer scheme [19]; we expect such an advantage to be preserved in the two-parameter optimal-transfer scheme.

The asymptotic results improve from the uniform chain ($x = y = 1$), which gives fidelity $\mathcal{F}_\infty = 1/2$, to the single tuned bond [15] ($y = 1$) giving $\mathcal{F}_\infty = 0.902$, and eventually to the optimal asymptotic fidelity evaluated in this paper, $\mathcal{F}_\infty = 0.991$. Whether comparable results could be obtained by other setups is difficult to say: the variants are numerous and we cannot give a conclusive word in this respect.

The quasiuniform channel here considered was previously used in Refs. [8,44] for the different purpose of exploiting the quasi-long-distance entanglement shared by the extremal spins in the ground state in order to get efficient teleportation; in those papers, proposals for realizing the model by means of coupled cavity arrays and ultracold atoms in 1D optical lattices are put forward. In the first proposal, each component of the array is made by an optical cavity with a two-level atom inside; by tuning the frequency of the cavity mode to an appropriate value, the effective qubit is given by the two lowest-lying degenerate energy levels of the field-dressed atom. Adjacent cavities can then be coupled by photon hopping or by waveguides: in the former case, the interaction strength is related to the overlap of the wave functions, so that increasing the displacements of the two cavities at each end would result in effective lower couplings; in the latter case, choosing waveguides with different dielectric properties would achieve the same result. The second proposal refers to bosonic ultracold atoms loaded in a one-dimensional optical lattice, which are well described by the Bose-Hubbard model. In the dynamical-parameter regime where the onsite repulsion is much larger than the hopping term, the Fock states with zero and one particle per site can be considered as the basis of a qubit and the Hamiltonian turns into an effective hopping model, like that of Eq. (1), with uniform couplings. Site-dependent couplings are then realized via local fields on single sites of the optical lattice, which give rise to an effective interaction between the sites adjacent to those with the local fields. The above physical realizations might possibly fit also our setup.

Finally, we mention the similarity between the problem of quantum-state transfer and the subject of continuous-time quantum walks [45], where regular spacetime structures called quantum carpets [46] can emerge from a complex dynamics: for instance, the revival of the wave function is analogous, in a mirror-symmetric context, to state transmission.

ACKNOWLEDGMENTS

We acknowledge financial support from the Italian Ministry of University in the framework of the 2008 PRIN program (contract N. 2008PARRTS 003). TJGA is supported by the European Commission, the European Social Fund and the Region Calabria through the program POR Calabria FSE 2007-2013-Asse IV Capitale Umano-Obiettivo Operativo M2. L. B. and P. V. gratefully thank Dr. A. Bayat and, with A. C., Professor S. Bose for useful discussions; T. J. G. A. thanks ISC-CNR for their kind hospitality.

APPENDIX A: SPECTRAL SOLUTION

1. Characteristic polynomial

The characteristic polynomial $\chi_N(\lambda; x, y) \equiv \det[\lambda - A(x, y)]$ associated with matrix (17) is

$$\chi_N(\lambda) = \begin{vmatrix} \lambda & -x & & & & & & \\ -x & \lambda & -y & & & & & \\ & -y & \lambda & -1 & & & & \\ & & -1 & \lambda & -1 & & & \\ & & & \ddots & \ddots & \ddots & & \\ & & & & -1 & \lambda & -y & \\ & & & & & -y & \lambda & -x \\ & & & & & & -x & \lambda \end{vmatrix}_N . \tag{A1}$$

Expanding $\chi_N(\lambda; x, y)$ in the last column, one finds

$$\chi_N = (\lambda^2 - x^2)\xi_{N-2} - \lambda y^2 \xi_{N-3}, \tag{A2}$$

where ξ_N is the characteristic polynomial of the associated matrix with only one nonuniform endpoint,

$$\xi_N(\lambda) = \begin{vmatrix} \lambda & -x & & & & & \\ -x & \lambda & -y & & & & \\ & -y & \lambda & -1 & & & \\ & & -1 & \lambda & -1 & & \\ & & & \ddots & \ddots & \ddots & \\ & & & & -1 & \lambda & -1 \\ & & & & & -1 & \lambda \end{vmatrix}_N , \tag{A3}$$

which can be expanded in the very same manner getting the analog of Eq. (A2),

$$\xi_N = (\lambda^2 - x^2)\eta_{N-2} - \lambda y^2 \eta_{N-3}, \tag{A4}$$

in terms of the characteristic polynomial $\eta_N(\lambda) \equiv \chi_N(\lambda; 1, 1)$ of the fully uniform matrix $A_N(1, 1)$. For η_N one has the recursion relation

$$\eta_N = \lambda \eta_{N-1} - \eta_{N-2}; \tag{A5}$$

together with the conditions $\eta_0 = 1$ and $\eta_1 = \lambda$, it can be solved in terms of Chebyshev polynomials of the second kind,

$$\eta_N = \frac{\sin(N+1)k}{\sin k}, \quad \lambda \equiv 2\cos k. \tag{A6}$$

Hence, in the uniform case the N solutions of the secular equation $\chi_N(\lambda; 1, 1) = \eta_N(\lambda) = 0$ correspond [47] to the following discrete values of k:

$$k = \frac{\pi n}{N+1}, \quad n = 1, \ldots, N. \tag{A7}$$

To extract the dependence on x and y in Eq. (A2) one first uses Eq. (A4),

$$\chi_N(\lambda) = (\lambda^2 - x^2)[(\lambda^2 - x^2)\eta_{N-4} - \lambda y^2 \eta_{N-5}] - \lambda y^2 [(\lambda^2 - x^2)\eta_{N-5} - \lambda y^2 \eta_{N-6}], \tag{A8}$$

and then Eq. (A6) in the form $\eta_N \sin k = \mathrm{Im}\{e^{i(N+1)k}\}$,

$$\chi_N(\lambda)\sin k = \mathrm{Im}\left\{(\lambda^2 - x^2 - \lambda y^2 e^{-ik})^2 e^{i(N-3)i}\right\} = \mathrm{Im}\left\{u_k^2 e^{i(N+1)k}\right\}, \tag{A9}$$

where

$$u_k \equiv (\lambda^2 - x^2 - \lambda y^2 e^{-ik})e^{-2ik} = 1 + (2 - x^2 - y^2)e^{-2ik} + (1 - y^2)e^{-4ik}. \tag{A10}$$

2. Shifts of eigenvalues

Equation (A9) leads to a compact expression of the secular equation, $\mathrm{Im}\{e^{i(N+1)k}u_k^2\} = 0$; in the fully uniform case, when both $x, y \to 1$, it has the solutions given by Eq. (A7). Setting

$$u_k \equiv |u_k| e^{-i\varphi_k}, \tag{A11}$$

the secular equation reads $\mathrm{Im}\{e^{i[(N+1)k-2\varphi_k]}\} = 0$, and the eigenvalues $\lambda_n = 2\cos k_n$ can be expressed as deviations from the uniform-case values (A7) due to the *phase shifts* φ_k,

$$k_n = \frac{\pi n + 2\varphi_{k_n}}{N+1}, \quad n = 1, \ldots, N. \tag{A12}$$

Keeping in mind that the variable k actually assumes the N discrete values $\{k_n\}$, one can unambiguously use the index k in the place of n. An explicit expression of the phase shifts follows immediately from Eq. (A10), by separating the real and imaginary parts of $u_k e^{2ik}$,

$$\varphi_k = 2k - \tan^{-1}\left[\frac{y^2 \sin 2k}{(2 - x^2 - y^2) + (2 - y^2)\cos 2k}\right]. \tag{A13}$$

3. Mode distribution

To evaluate the transition amplitude (16) one needs the square components of the first column of the orthogonal matrix U defined by Eq. (2). A nice formula derived in Ref. [42] (Corollary 7.9.1) helps: with the formalism used here it reads

$$\mathcal{P}_n \equiv U_{n1}^2 = \frac{\chi_{2:N}(\lambda_n)}{\partial_\lambda \chi_N(\lambda_n)}, \tag{A14}$$

where $\chi_{2:N}(\lambda)$ is the first minor of the determinant (A1). It is equivalent to using the variable $k = \cos^{-1}\frac{\lambda}{2} \in (0, \pi)$ and writing

$$\mathcal{P}_k \equiv U_{k1}^2 = -2\sin k \frac{\chi_{2:N}(k)}{\partial_k \chi_N(k)}, \tag{A15}$$

with k definitely taking the allowed values (A12) [i.e., $\chi_N(k) = 0$]. As $\chi_{2:N}(\lambda) = \lambda\xi_{N-2} - y^2\xi_{N-3}$, with calculations similar to those which lead to Eq. (A9), it is found that

$$\chi_{2:N}(k)\sin k = \mathrm{Im}\{e^{iNk}u_k v_k\}. \tag{A16}$$

with

$$v_k = 1 + (1 - y^2)e^{-2ik}. \tag{A17}$$

By deriving Eq. (A9) with respect to k one has

$$\sin k\,\partial_k \chi_N(k) = \mathrm{Im}\left\{e^{i(N+1)k}\left[i(N+1)u_k^2 + 2u_k u_k'\right]\right\} = (N+1)\mathrm{Re}\left\{e^{i(N+1)k}u_k^2\right\} + 2\mathrm{Im}\left\{e^{i(N+1)k}u_k u_k'\right\}. \tag{A18}$$

The argument of Re is real by the secular equation so, using $u_k'/u_k = \partial_k \ln u_k = \partial_k \ln|u_k| - i\varphi_k'$,

$$\sin k\,\partial_k \chi_N(k) = \left[N + 1 + 2\mathrm{Im}\left\{\frac{u_k'}{u_k}\right\}\right] e^{i(N+1)k}u_k^2 = (N + 1 - 2\varphi_k')e^{i(N+1)k}u_k^2. \tag{A19}$$

Equation (A15) becomes

$$\mathcal{P}_k = -\frac{2\sin k}{N+1-2\varphi_k'}\frac{\mathrm{Im}\{e^{iNk}u_k v_k\}}{e^{i(N+1)k}u_k^2} = \frac{2\sin k}{N+1-2\varphi_k'}\frac{\mathrm{Im}\{e^{ik}u_k v_k^*\}}{|u_k|^2}. \tag{A20}$$

By means of Eqs. (A10) and (A17) one can express $u_k = v_k(1 + e^{-2ik}) - x^2 e^{-2ik}$, and a simple expression of the numerator follows: $\mathrm{Im}\{e^{ik}u_k v_k^*\} = x^2 y^2 \sin k$, finally yielding

$$\mathcal{P}_k = \frac{2x^2y^2}{N+1-2\varphi_k'}\frac{\sin^2 k}{|u_k|^2}. \tag{A21}$$

A manageable expression for $|u_k|^2$ arises by working out Eq. (A10),

$$e^{2ik}u_k = -x^2 + 2(2 - y^2)\cos^2 k + 2iy^2 \sin k \cos k, \tag{A22}$$

and taking the square modulus. After some algebra, the outcome is

$$\mathcal{P}_k = \frac{2x^2y^2}{N+1-2\varphi_k'} \times \frac{1}{x^4 + (4 - x^2 - 2y^2)^2\cot^2 k - 16(1 - y^2)\cos^2 k}. \tag{A23}$$

An explicit expression for φ_k' can be found going back to Eq. (A19)

$$\varphi_k' = -\mathrm{Im}\left\{\frac{u_k'}{u_k}\right\} = -\frac{\mathrm{Im}\{u_k^* u_k'\}}{|u_k|^2}, \tag{A24}$$

where, from Eq. (A10),

$$u_k' = -2i[u_k - 1 - (1 - y^2)e^{-4ik}], \tag{A25}$$

and some further calculation gives

$$|u_k|^2\varphi_k' = 2\mathrm{Re}\{u_k^*[u_k - 1 - (1 - y^2)e^{-4ik}]\} = 2|u_k|^2 - 2y^2[x^2 + 2(2 - x^2 - y^2)\cos^2 k]. \tag{A26}$$

Eventually, the mode density can be made fully explicit starting again from Eq. (A21),

$$\mathcal{P}_k = \frac{2x^2y^2\sin^2 k}{(N-3)\{[x^2 - 2(2 - y^2)\cos^2 k]^2 + 4y^4\cos^2 k \sin^2 k\} + 4y^2[x^2 + 2(2 - x^2 - y^2)\cos^2 k]}. \tag{A27}$$

[1] J. I. Cirac and P. Zoller, Phys. Rev. Lett. **74**, 4091 (1995).
[2] A. Blais, R.-S. Huang, A. Wallraff, S. M. Girvin, and R. J. Schoelkopf, Phys. Rev. A **69**, 062320 (2004).
[3] C.-P. Yang, Phys. Rev. A **82**, 054303 (2010).
[4] V. Pouthier, e-print arXiv:1201.5184.
[5] H.-J. Briegel, T. Calarco, D. Jaksch, J. I. Cirac, and P. Zoller, J. Mod. Opt. **47**, 415 (2000).
[6] J. F. Sherson, C. Weitenberg, M. Endres, M. Cheneau, I. Bloch, and S. Kuhr, Nature (London) **467**, 68 (2010).
[7] E. H. Lapasar, K. Kasamatsu, Y. Kondo, M. Nakahara, and T. Ohmi, J. Phys. Soc. Jpn. **80**, 114003 (2011).
[8] S. M. Giampaolo and F. Illuminati, New J. Phys. **12**, 025019 (2010).
[9] G. M. Nikolopoulos, D. Petrosyan, and P. Lambropoulos, J. Phys.: Condens. Matter **16**, 4991 (2004).
[10] D. Petrosyan and P. Lambropoulos, Opt. Comm. **264**, 419 (2006).
[11] S. Paganelli, G. L. Giorgi, and F. de Pasquale, Fortschr. Phys. **57**, 1094 (2009).
[12] S. Yang, A. Bayat, and S. Bose, Phys. Rev. A **82**, 022336 (2010).
[13] S. Bose, Phys. Rev. Lett. **91**, 207901 (2003).
[14] S. Bose, Contemp. Phys. **48**, 13 (2007).
[15] L. Banchi, T. J. G. Apollaro, A. Cuccoli, R. Vaia, and P. Verrucchi, New J. Phys. **13**, 123006 (2011).
[16] A. Bayat and S. Bose, Phys. Rev. A **81**, 012304 (2010).
[17] A. Bayat, L. Banchi, S. Bose, and P. Verrucchi, Phys. Rev. A **83**, 062328 (2011).
[18] L. Banchi, A. Bayat, P. Verrucchi, and S. Bose, Phys. Rev. Lett. **106**, 140501 (2011).
[19] A. Zwick, G. A. Álvarez, J. Stolze, and O. Osenda, Phys. Rev. A **85**, 012318 (2012).
[20] M. Rafiee, M. Soltani, H. Mohammadi, and H. Mokhtari, Eur. Phys. J. D **63**, 473 (2011).
[21] M. L. Hu, Eur. Phys. J. D **64**, 531 (2011).
[22] A. Kay, Int. J. Quantum Inform. **8**, 641 (2010).
[23] P. Karbach and J. Stolze, Phys. Rev. A **72**, 030301 (2005).
[24] M. Christandl, N. Datta, A. Ekert, and A. J. Landahl, Phys. Rev. Lett. **92**, 187902 (2004).
[25] M.-H. Yung and S. Bose, Phys. Rev. A **71**, 032310 (2005).
[26] C. Di Franco, M. Paternostro, and M. S. Kim, Phys. Rev. Lett. **101**, 230502 (2008).
[27] A. Zwick, G. A. Álvarez, J. Stolze, and O. Osenda, Phys. Rev. A **84**, 022311 (2011).
[28] Y. Wang, F. Shuang, and H. Rabitz, Phys. Rev. A **84**, 012307 (2011).
[29] M. Bruderer, K. Franke, S. Ragg, W. Belzig, and D. Obreschkow, Phys. Rev. A **85**, 022312 (2012).
[30] P. Cappellaro and L. Viola, and C. Ramanathan, Phys. Rev. A **83**, 032304 (2011).
[31] C. Ramanathan, P. Cappellaro, L. Viola, and D. G. Cory, New J. Phys. **13**, 103015 (2011).
[32] A. Wójcik, T. Łuczak, P. Kurzyński, A. Grudka, T. Gdala, and M. Bednarska, Phys. Rev. A **72**, 034303 (2005).
[33] T. J. G. Apollaro and F. Plastina, Phys. Rev. A **74**, 062316 (2006).
[34] L. Campos Venuti, C. Degli, Esposti Boschi, and M. Roncaglia, Phys. Rev. Lett. **99**, 060401 (2007).
[35] L. Banchi, T. J. G. Apollaro, A. Cuccoli, R. Vaia, and P. Verrucchi, Phys. Rev. A **82**, 052321 (2010).
[36] E. B. Fel'dman, E. I. Kuznetsova, and A. I. Zenchuk, Phys. Rev. A **82**, 022332 (2010).
[37] A. Zwick and O. Osenda, J. Phys. A **44**, 105302 (2011).
[38] N. Y. Yao, L. Jiang, A. V. Gorshkov, Z.-X. Gong, A. Zhai, L.-M. Duan, and M. D. Lukin, Phys. Rev. Lett. **106**, 040505 (2011).
[39] T. J. Osborne and N. Linden, Phys. Rev. A **69**, 052315 (2004).
[40] H. Yadsan-Appleby and T. J. Osborne, Phys. Rev. A **85**, 012310 (2012).
[41] D. L. Aronstein and C. R. Stroud, Phys. Rev. A **55**, 4526 (1997).
[42] B. N. Parlett, *The Symmetric Eigenvalue Problem* (SIAM, Philadelphia, 1998).
[43] A. Cantoni and P. Butler, Linear Algebra Appl. **13**, 275 (1976).
[44] S. M. Giampaolo and F. Illuminati, Phys. Rev. A **80**, 050301 (2009).
[45] O. Mülken and A. Blumen, Phys. Rev. E **71**, 036128 (2005).
[46] W. Kinzel, Physikalische Blätter **51**, 1190 (1995).
[47] E. Lieb, T. Schultz, and D. Mattis, Ann. Phys. (NY) **16**, 407 (1961).